Journal of Applied Electrochemistry **33**: 541–547, 2003.

Electrocatalytic hydrogenation of cyclohexanone: Simple dynamic cell design

P. DUBÉ[1], F. KERDOUSS[2], F. LAPLANTE[1], P. PROULX[2], L. BROSSARD[3,*] and H. MÉNARD[1]
[1]*Département de Chimie, Université de Sherbrooke, Sherbrooke (Québec), Canada J1K 2R1*
[2]*Faculté de Génie, Centre de Recherche de Technologie des Plasmas, Université de Sherbrooke, Sherbrooke (Québec), Canada J1K 2R1*
[3]*Institut de Recherche d'Hydro-Québec (IREQ) 1800 boul. Lionel-Boulet, Varennes (Québec), Canada J3X 1S1 (* author for correspondence, e-mail: brossard.louis@ireq.ca)*

Received 18 June 2002; accepted in revised form 18 February 2003

Key words: catalysis, dynamic cell, electrochemistry, electrohydrogenation

Abstract

The electrocatalytic hydrogenation of cyclohexanone has been investigated with catalytic powder particles made of metal nanoaggregates deposited on a nonconductive material such as activated carbon and alumina. The catalytic powder particles were suspended in the solution under vigorous stirring conditions. The brief contact of the powder particles with a porous carbon cathode was sufficient to form adsorbed hydrogen on the metallic nanoaggregates through water electrolysis and initiate the electrohydrogenation process. It is demonstrated that the key parameters of the electrohydrogenation process are both the nature of the metallic nanoaggregates and the nature of the nonconductive material. The hydrodynamics of the solution under vigorous stirring conditions have also been studied for the particular cell used in the present study.

1. Introduction

Currently, hydrogenation is used on a very large scale industrially; for example, it is estimated [1] that in 1990, more than 35% of all catalysts produced in the United States were used for hydrogenation of petrochemicals. In conventional hydrogenation, hydrogen gas is dissociated into atoms on the surface of an active metal such as palladium, platinum, rhodium, ruthenium or Raney nickel, which is deposited on a matrix of large surface area, such as alumina, silica or a zeolite. Conditions are often vigorous (pressures up to 500 atm and temperatures up to 200 °C), leading to problems such as expensive reactor design and to thermal decomposition, isomerization or polymerization of some organic substrates.

Electrocatalytic hydrogenation offers a method of carrying out the same reactions at ambient temperature and pressure, by producing hydrogen atoms at a cathode through electrolysis of water [2, 3]. The method is applicable to hydrogenation of all kind of unsaturated molecules, including aromatics and carbonyl compounds [4]. In an alkaline solution, the overall electrode reaction involves several steps as illustrated below.

$$H_2O + e^- + M \rightarrow M(H) + OH^- \quad (1)$$

$$Y{=}CZH + A \underset{K_{des}}{\overset{K_{ads}}{\rightleftharpoons}} (Y{=}CZH)A \quad (2)$$

$$(Y{=}Z)A + M(H) \rightarrow (YH{-}ZH)A + M \quad (3)$$

$$(YH{-}ZH)A \underset{K_{ads}}{\overset{K_{des}}{\rightleftharpoons}} YH{-}ZH + A \quad (4)$$

$$2\,M(H) \rightarrow H_{2(g)} + M \quad (5)$$

$$M(H) + H_2O + e^- \rightarrow H_{2(g)} + OH^- + M \quad (6)$$

First, the hydrogen is generated through an electrochemical reaction (Equation 1) on metallic sites (M). In addition, a nonconductive material (A) is used for the adsorption of the organic molecules (Equation 2). Further, adsorbed hydrogen and organic molecules react together at the electrode surface to generate a new organic molecule richer in hydrogen (Equation 3.1). Reaction 3 is followed by the desorption of freshly generated organic molecules, as illustrated in Equation 4. It should be noted that a fraction of H_{ads} generated from Reaction 1 is not used for the electrohydrogenation process, but rather for the generation of molecular hydrogen through step 5 or 6. Since steps 1 to 6 are surface reactions, the nature of both the metal and the non conductive material at the solution–electrode interface may play a key role in the reaction kinetics.

In the past, solid electrodes of catalytic metals and the matrix pressed together were used [4]. More recently, a

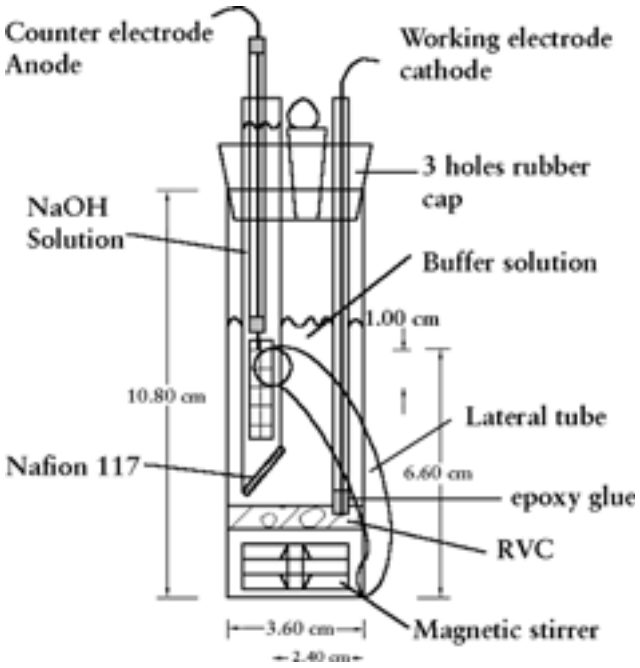

Fig. 1. Schematic of the electrochemical cell.

new electrode approach was considered [5]. It consists of a plate of very porous carbon as the electronic conductor, with a catalytic powder being trapped or agglomerated on the carbon plate. Powder catalysts are in the form of very small metallic particles deposited on larger nonconductive material particles. Metallic particles are dispersed on the matrix in different ways [6], that is, physical vapour deposition, impregnation or chemical vapour deposition. As far as the electrohydrogenation process is concerned, an H cell is used; the catalyst powder is agglomerated to perform hydrogenation. In the present paper, a different cell design is considered (Figure 1). This cell configuration allows the catalytic powder to flow through the reticulated vitreous carbon electrode (RVC). The electrode seems to work like a fluidized bed or could be compared to a current pulse electrochemical reaction. This allows the catalyst to be in an open circuit condition when it is circulating in the cell and in an applied current state when it is flowing in the electrode. Monoatomic hydrogen is produced only in the electrode core when current is applied. When the catalyst is in an open circuit mode, atomic hydrogen favours the hydrogenation of organic molecules instead of diatomic hydrogen production because the Tafel hydrogen evolution reaction cannot proceed. For these reasons, it is probable that electrohydrogenation efficiency is increased compared to a constant current method.

2. Experimental details

The counter-electrode (i.e., the anode) was built from a glass tube with an internal diameter of one-half inch; one end of the tube was cut at an angle of about 45° to avoid any further hydrogen accumulation under the counter-electrode membrane. On the bevel side, a 5 min drying epoxy glue was spread over and covered immediately by a Nafion®117 membrane piece. The size of the membrane was adjusted to the bevel size prior to coating the junction, between the glass and Nafion®, with a layer of epoxy to prevent any liquid from seeping out. The counter electrode was made of stainless steel or platinum wire gauze.

The working electrode was made from a foil of reticulated vitreous carbon one-half inch thick and with 100 ppi (pores per linear inch). The electrochemical cell was used like a punch to cut an electrode disc in the reticulated vitreous carbon, the diameter of the disc and the cell being the same. The resulting disc was cut in two parts each one-quarter inch thick. A copper wire 18 cm in length with both ends buffed was introduced in a 15 cm long glass tube. One end of the wire was cut at angle; the end of the glass tube was filled with epoxy and the copper wire was introduced to a 3 mm depth in the reticulated vitreous carbon cylinder made earlier (after which the glass tube was introduced to the same depth). The other side of the tube was sealed with epoxy glue to prevent the solvent from rising up the tube.

Stirring of the solution was achieved using a star head magnetic stirrer 3.02 cm × 1.27 cm. The head of the cell was a rubber cap in which three holes were drilled: one for the counter-electrode compartment, one for the working electrode glass rod and one for the sampling.

2.1. *Products and materials*

The following materials and chemicals were used: reticulated vitreous carbon 100 ppi, one-half inch thick plate (Electrosynthesis Co.); potassium phosphate, monohydrate, ACS grade (Anachemia), sodium hydroxide, ACS (BDH), rhodium 5 wt % on alumina powder, platinum 5 wt % on alumina powder, platinum 5 wt % on activated carbon, palladium 5 wt % on alumina powder and palladium 5 wt % on activated carbon (Aldrich), rhodium 5 wt % on activated carbon, ruthenium 5 wt % on reduced alumina powder and ruthenium 5 wt % on activated carbon (Alfa); nickel 10 wt % in graphite, Graphimet Ni-10 (Johnson Matthey Electronic). In addition, a star head magnetic stirrer (Fisher Scientific) was used to stir the electrolyte.

2.2. *Procedure*

The cell contained 60 mL of a phosphate buffer at pH 7 (KH_2PO_4 + NaOH). The rotation speed of the stirrer was about 800 rpm. The stirring action must be sufficiently vigorous otherwise the liquid flow rate in the ankle (lateral tube) was too low to allow catalyst particle displacement in the tube. A modelling of the flow is illustrated in Figure 5. After the addition of 200 mg of powder catalyst into the solution, the rubber cap and the two electrodes were installed on the cell. Air bubbles trapped under the reticulated vitreous carbon electrode were removed by moving the electrode up and down.

The electrode was polarized for 2 h under an applied constant current of 5 mA, with the corresponding charge being 30 C. The polarization time was long enough to allow the particles to reach a steady-state regime in such a way that they are momentarily trapped in the pores of the working electrode so that atomic hydrogen generation occurred. After polarization, 1 mL of cyclohexanone solution (0.25 M) in water was poured in the cell. 1 mL of solution was removed and a constant current of 20 mA was applied. Samples of 1 mL of solution were removed at different times during the electrolysis. Cyclohexanone and cyclohexanol were extracted in ethyl acetate using the following procedure: five drops of HCl + 100 mg NaCl + 100 μL ISTD (3-methylcyclohexanol 0.02 M in water) + 1 mL of ethyl acetate were shaken together and allowed to settle. The aqueous phase was frozen on an acetone/CO_2 ice mix. The organic part was removed and dried in a pasteur pipet containing glass wool and Na_2SO_4. A 100 μL ESTD (cyclohexen-1-one 0.02 M in ethyl acetate) was added to the organic phase and injected in a gas chromatograph (DB-5 column, oven at 90 °C, injector at 250 °C and FID detector at 300 °C) to further identify the organic compounds.

3. Mathematical modelling of the cell

To better understand and improve cell performance, a model was developed to predict the flow fields inside the cell. The model is based on the commercial computational fluid dynamics (CFD) code Fluent^{TM}. The capabilities of this code enable us to model geometrically the cell in a very accurate way by use of the nonstructured grids. A detailed description of the mathematical and numerical techniques used in Fluent^{TM} is beyond the scope of the present paper although we will summarize it in the following Section.

3.1. *Mathematical model*

3.1.1. *Reynolds averaged Navier–Stokes equations*

Turbulent flows are characterized by fluctuating velocity fields. These fluctuations mix transported quantities such as momentum, energy, and species concentration, and cause the transported quantities to fluctuate. Since these fluctuations can be of small scale and high frequency, they are too computationally expensive to simulate directly in practical engineering calculations. Instead, the instantaneous (exact) governing equations can be averaged, or otherwise manipulated to remove the small scales, resulting in a modified set of equations that are computationally less expensive to solve. In Reynolds averaging, the solution variables in the instantaneous (exact) Navier–Stokes equations are decomposed into the mean and fluctuating components. For the velocity components:

$$u_i = \bar{u}_i + u_i'$$

where $\bar{u}_i$ and u_i' are the mean and fluctuating velocity components ($i = 1, 2, 3$) and i represent the coordinate system.

Substituting expressions of this form for the flow variables into the instantaneous continuity and momentum equations and taking an average and dropping the overbar on the mean velocity yields the ensemble-averaged continuity and momentum equations. They can be respectively written in Cartesian tensor form, for steady state flow, as

$$\frac{\partial(\rho u_i)}{\partial x_i} = 0.0$$

$$\frac{\partial(\rho u_i u_j)}{\partial x_i} = -\frac{\partial p}{\partial x_i} + \frac{\partial}{\partial x_j}\left[\mu\left(\frac{\partial u_i}{\partial x_j} + \frac{\partial u_j}{\partial x_i}\right)\right] + \frac{\partial(-\rho\overline{u_i' u_j'})}{\partial x_j} + S_i$$

These two equations are called Reynolds-averaged Navier–Stokes (RANS) equations. They have the same general form as the instantaneous Navier–Stokes equations, with the velocities and other solution variables now representing averaged values. Additional terms now appear that represents the effects of turbulence. This Reynolds stresses tensor $-\rho\overline{u_i' u_j'}$ must be modelled to close the momentum equation. We use the Reynolds stress model (RSM) to solve transport equations for each of the terms in the Reynolds stress tensor. This model is used with the standard wall functions that are a collection of semi-empirical formulas and functions that link the solution variables at the near wall cells and the corresponding quantities on the wall. ρ, p and μ represent, respectively, density, pressure and viscosity of the fluid, S_i represents external body forces or frame forces and also contains other model-dependent source terms such as porous-media.

3.1.2. *Darcy's law modelling of the porous media*

The porous media model incorporates an empirically determined flow resistance in a region of the model defined as the porous zone. The porous media model involves an added momentum sink S_i in the governing momentum equations in that zone. The sink term S_i is a viscous loss term (Darcy term) contributing to the pressure gradient in the porous cell and creating a pressure drop that is proportional to the fluid velocity in the cell. The sink term S_i is written for simple homogeneous porous media as

$$S_i = -\frac{\mu}{\alpha} u_i$$

where α is the porosity of the media.

3.1.3. *Multiple reference frame representing the magnetic rotor at the bottom of the cell*

The solution of flows in moving reference frames induced by the magnetic rotor requires the use of moving cell zones. This cell zone motion is interpreted as the motion of a reference frame to which the cell zone is

attached. In this situation, the acceleration of the coordinate system is included in the equations of motion describing the flow. In Fluent^{TM}, we use 'multiple reference frame' (MRF) including a rotating frame of reference attached to the magnetic rotor and a stationary frame of reference attached to the rest of the cell model.

In the rotating frame, an additional term, $\vec{S}$, appears in the momentum equation including the Coriolis and centrifugal accelerations:

$$\vec{S} = -2 \cdot \rho(\vec{\omega} \times \vec{v}_r) - \rho \cdot \vec{\omega} \times (\vec{\omega} \times \vec{r})$$

where $\vec{\omega}$ is the angular velocity vector, $\vec{v}_r$ is the relative velocity and $\vec{r}$ is the position vector in the rotating frame.

3.2. *Numerical technique*

This consisted of: a nonstructured mesh adapted to the geometry (Figure 2), a second order scheme as descretization scheme and an iterative uncoupled solution to the discrete form of the mathematical model using a simple algorithm for pressure–velocity coupling.

Figure 2 shows the essential features of the unstructured grid that models the geometry of the cell. This unstructured mesh was used to discretize the cell in order to convert the governing equations of continuity and momentum to algebraic equations that can be solved numerically. Figure 2 also shows the various zones of the cell including the main body, the two electrodes, the porous carbon fibre zone, the magnetic stirrer and the (lateral) tube.

3.3. *Results of the numerical modelling*

The solution of the cell model with its boundary conditions enables confirmation of the features that were noted in the experimental cell. Figures 3 and 4 show the velocity magnitude vectors on a cross-section of the cell at the level of the magnetic stirrer. In Figure 3, the results are obtained in terms of velocity magnitude vector created by the magnetic rotor as a function of rotation speed. When the magnetic stirrer rotates in a clockwise direction – obviously the most efficient way to operate the cell – the fluid is pushed by the stirrer directly into the opening and flow separation in the lateral tube is minimized. On the other hand, as shown in Figure 4, when the rotation is reversed, a significant separation is observed that makes the recirculation flowrate decrease significantly.

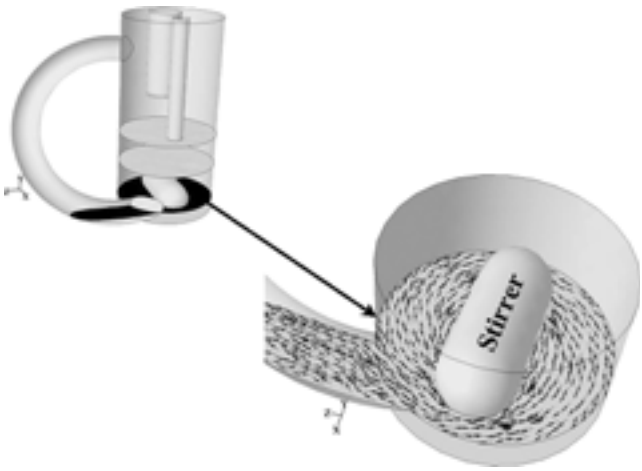

Fig. 3. Vector plots showing the velocity fields obtained at the bottom of the cell with clockwise rotation.

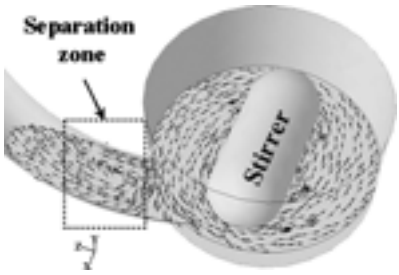

Fig. 4. Vector plots showing the velocity fields obtained at the bottom of the cell with counter-clockwise rotation.

The results shown in Figures 3 and 4 represent the flow patterns at 800 rpm. The simulations were obtained from 100 to 800 rpm, and the overall results shown in terms of flowrates (in the lateral tube) against the rotation rates are given in Figure 5. As anticipated from

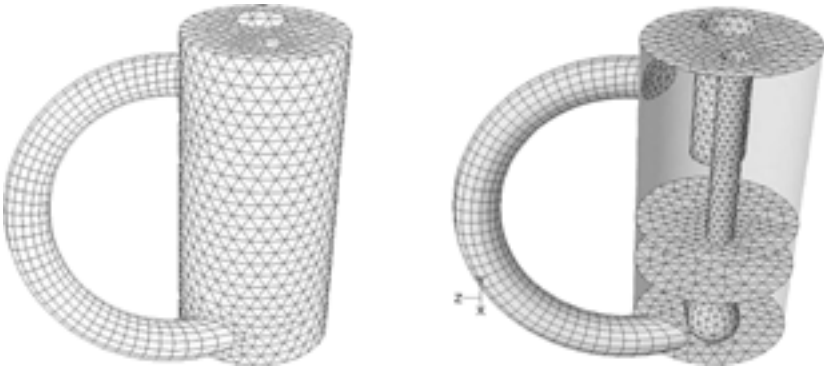

Fig. 2. Non-structured grid model of the cell showing the various zones.

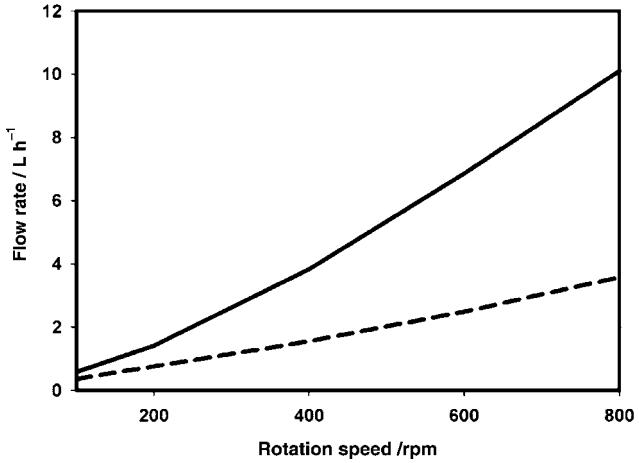

Fig. 5. Circulation flow rates in the lateral tube as function of the rotation speed. Key: (——) clockwise rotation; (– – –) counter clockwise rotation.

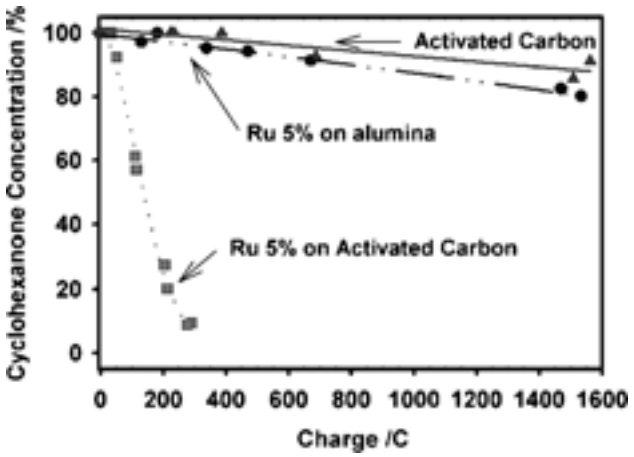

Fig. 6. Electrohydrogenation of cyclohexanone on a ruthenium catalyst.

Figures 3 and 4, the flowrate is reduced by a factor of 3 for a counter-clockwise rotation compared to clockwise rotation. Moreover, the relationship between the flowrate and the rotation rate is not linear, but has a power-law characteristic. We have demonstrated the ability of CFD modelling to study the hydrodynamics in an electrocatalytic cell. Further research continues in order to implement an electrochemistry model of the dynamic cell within CFD code.

4. Results and discussion

The electrohydrogenation process was carried out using various catalysts. All the experiments were carried out twice for data reproducibility reasons. In a first set of experiments, the electrohydrogenation was investigated on bare activated carbon to test the reactivity of the base support. As shown, as an example, in Figure 6, the activated carbon, which is a very strong adsorbent of organic molecules, is not active toward the hydrogenation of cyclohexanone; which is attributed to the high hydrogen overpotential on this material. Consequently, it is anticipated that active carbon must be used in conjunction with deposited metals to favour the atomic hydrogen generation on the metallic sites, the electrohydrogenation being induced by further reaction between the adsorbed hydrogen on metal and adsorbed organic molecules on alumina or activated carbon. The metals considered were ruthenium (Figure 6), platinum, rhodium and palladium. Two different matrix materials were considered: activated carbon and alumina. The ratio of unreacted cyclohexanone on its initial amount in the electrolyte is given in Table 1 for the different materials used.

As far as the cyclohexanone electrohydrogenation process is concerned, the electrocatalytic activity of metals dispersed on alumina particles decreases in the order: Rh > Pt = Pd > Ru. The ability of a metal to promote electrohydrogenation or hydrogenation catalysis of a specific type of bond is not well understood. In a catalytic hydrogenation process, the most extended theory which explains a metal's activity is based on both the adsorption heat of H_2 on the metal and the dissociation energy of the adsorbed molecular hydrogen into atomic hydrogen. The adsorption of organic molecules on the metal, by way of the electrons in π bonds, is justified by the presence of an empty d-orbital on the metal surface. The selectivity of metals and their supports toward the hydrogenation of ketone, aldehyde, aromatic ring, nitrile, carboxylic acid and other organic chemical functions have been extensively investigated [7, 8]. Metal activity is well known but there is no physical theory to explain the selectivity by way of molecular hydrogen energy of adsorption and organic adsorption energy or π bond energy. The support matrix plays a structural role for monocrystallites metal and gives a

Table 1. Unreacted cyclohexanone after 3 equivalents* (150 C) and 7 equivalents* (350 C)

Metal	Support		
	Alumina 350 C	Activated carbon 150 C	Graphite 350 C
Platinum	88%	5%	–
Palladium	88%	84%	–
Ruthenium	96%	40%	–
Rhodium	5%	5%	–
Nickel	–	–	15%

*One equivalent is the minimal charge required for the complete hydrogenation of the cyclohexanone dissolved in the electrolyte.

large specific area for metal deposition. The supporting matrix can also modify the adsorption energy of atomic hydrogen on metal through the effect of the matrix empty d-orbital [9]. These orbitals can strengthen or weaken the M–H bond and change the activity of the catalytic powder.

In the electrocatalytic hydrogenation process, where atomic hydrogen is produced on metal by water electrolysis, the two key parameters are the kinetics of water electroreduction to hydrogen gas on a selected metal (characterized by η, the overpotential at 10 mA cm^{-2}) and the strength of the hydrogen–metal bond (described by ΔH_{ads}, the adsorption enthalpy of hydrogen on the metal). The adsorption enthalpy is related to the strength of the chemisorption between the hydrogen adsorbed and the metal. These two parameters are given in the volcano curve (Figure 7) for different metals [10]. The less negative value of η is for the most active metals toward H_2 formation. From Figure 7, it may be deduced that the metals studied in this paper have similar activity for hydrogen chemisorption (all the values of ΔH_{ads} are situated between −260 and −270 kJ mol^{-1}). From the mechanisms described by Equations 5 and 6, the hydrogen evolution, a part of H_{ads}, could not be used for the electrocatalytic hydrogenation of organic molecules, the organic molecules being principally adsorbed on the non conductive material. Consequently, the greater the adsorption of organic molecules, the larger the number of organic molecules to be hydrogenated at the matrix–solution interface, with the result that the kinetics of the transfer of a monoatomic hydrogen (H_{ads}) from the metal site to an electron of the π-bond of the adsorbed organic molecule would be increased (Equation 3). The comparison of the performance obtained between a very strong adsorbent matrix (activated carbon) and a moderate adsorbent (alumina) could give qualitative information about this matter. If the kinetics of Equation 3 is faster than those of Equations 5 and 6, hydrogenation would be favoured compared to hydrogen evolution reaction and the performance would be increased.

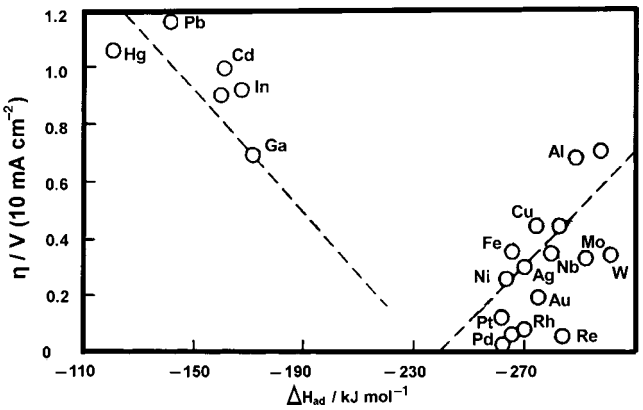

Fig. 7. Volcano-curve characterizing the catalytic activity of different metals for H_2 evolution (η, hydrogen overpotential at 10 mA cm^{-2}) [10].

As shown in Table 1, on an activated carbon matrix, the electrocatalytic activity decreases in the following order: rhodium > platinum > ruthenium > palladium. Rhodium is a very good metal catalyst for the hydrogenation of ketones because it shows the same activity in the presence of both adsorbents. In this case, the reaction rate corresponding to Equation 3 should be very fast compared to the hydrogen evolution reaction. The hydrogenation reaction is then limited by the amount of adsorbed hydrogen, as higher concentrations of organic molecules at the electrode–liquid interface do not significantly increase the hydrogenation performance. In the case of platinum, a good electrocatalyst for H_2 formation, when organic molecules are found in a large concentration near the metal clusters (with an activated carbon matrix), electrohydrogenation is favoured. In the present study ruthenium is one of the least active metals toward hydrogen evolution; it should therefore be attractive for cyclohexanone hydrogenation. However, experimental data show the reverse trend. For this metal, monoatomic hydrogen transfer from metal to adsorbed organic molecules (Equation 3) should be the limiting step of the reaction and the kinetics of the hydrogenation step of the organic molecules should benefit from an increase of the organic molecule concentration at the catalyst-solution interface. The electrohydrogenation activity of ruthenium is improved by the change in the matrix composition; the carbon catalyst shows a performance twice as great as the alumina catalyst (Figure 6). As compared to the other metal catalysts, palladium is always the least active. The above observations are attributed to the kinetics of hydrogen evolution and the hydrogen transfer process. Palladium is the most active metal toward the hydrogen evolution reaction (Volcano curve). For this reason, the generation rate of H_2 through Reactions 5 and 6 may be favoured. From the results obtained here, it appears that the rate of the hydrogen transfer from metals to organic molecule π-bonds (Equation 3) is slower than the other metals studied. The hydrogen evolution reaction rate could be faster than Reaction 3. So, an increase in the concentration of organic molecules (with the use of activated carbon) near the metal leads to improved hydrogenation performance but the kinetics of Reaction 3 do not seem to occur as effectively as the hydrogen evolution rate. The physical explanation in this case is not yet known but only observed [4]. Nickel seems to be good for the electrohydrogenation of ketone but it could not be compared with the other catalysts because of the metal concentration and the type of matrix. Nickel on alumina or activated carbon is not available commercially.

5. Conclusion

The ECH of cyclohexanone to cyclohexanol is largely dependant on the nature of both the metal nanoaggregates dispersed on a nonconductive matrix particle and

the matrix particle. The ECH is improved by the use of activated carbon as the matrix material compared to alumina; for both matrix materials, the best performances are observed with Rh nanoaggregates. It is deduced that the use of a very strong adsorbent matrix material for organic molecules, that is, activated carbon, is better than the use of a moderate absorbent, that is, alumina.

Acknowledgements

The authors gratefully acknowledge the Fonds Canadien pour l'Avancement de la Recherche (FCAR) and the National Research Council of Canada for their financial support.

References

1. J.A. Kent, 'Reigel's Handbook of Industrial Chemistry' (Chapman & Hall, London, 9th edn, 1992), p. 451.
2. W.M. Leslie and J.A.V. Butler, *Trans. Faraday Soc*. **32** (1936), 989.
3. J.M. Chapuzet, A. Lasia and J. Lessard, *in* J. Lipkowski and P.N. Ross (Eds), *Electrocatalysis* (Wiley–VCH, New York, 1998), p. 155.
4. K. Amouzegar and O. Savadogo, *J. Appl. Electrochem*. **27** (1997) 539.
5. P. Dabo, F. Laplante, J. Lessard, L. Brossard and H. Ménard, *Env. Sci. Technol*. **37** (2000) 1265.
6. B.S. Kang, *J. Mater. Sci*. **30** (1995) 3883.
7. Y. Huang and W.M.H. Sachtler, *Appl. Catal. A* **182** (1999) 365.
8. R. Jaganathan, V.G. Ghugikar, R.V. Gholap, R.V. Chaudhari and P.L. Mills, *Ind. Eng. Chem. Res*. **38** (1999) 4634.
9. J.B. Moffat, 'Theoretical aspects of Heterogeneous Catalysis' (Van Nostrand Reinhold, New York, 1990), p. 360.
10. H. Wendt, 'Electrochemical Hydrogen Technologies' (Elsevier, Amsterdam, 1990), p. 18.